J Mater Sci (2007) 42:3033–3043
DOI 10.1007/s10853-006-0532-7

The influence of calcium content on the structure and thermal performance of fly ash based geopolymers

K. Dombrowski · A. Buchwald · M. Weil

Received: 5 September 2005 / Accepted: 6 June 2006 / Published online: 30 December 2006

Abstract The influence of calcium and its content on the structure formation, hardening, and performance of fly ash based geopolymeric binder was the objective of our investigation. Calcium hydroxide was added to fly ash in different amounts. Since it is known that the formed structure determines certain properties of the material, the coherence between different types and various ratios of the reaction products on thermal properties such as strength after thermal treatment up to 1,100 °C, thermal resistance under load, creep in compression, and axial dilation were investigated. The results were compared to the type and composition of the reaction product, which was detected, for example, by ^{29}Si NMR spectroscopy and X-ray diffraction. Along with calcium containing zeolitic phases, the calcium built C–S–H-phases using the silicon from the fly ash, both of which crystallize or convert into new phases at elevated temperatures.

K. Dombrowski
Institute of Ceramic, Glass and Construction Materials, Technical University Bergakademie Freiberg, Freiberg, Germany

A. Buchwald (✉)
Bauhaus-University Weimar, Coudraystr. 13C, Weimar 99421, Germany
e-mail: anja.buchwald@bauing.uni-weimar.de

M. Weil
Department of Technology-Induced Material Flow (ITC-ZTS), Forschungszentrum Karlsruhe, Karlsruhe, Germany

Introduction

The demands on modern building materials arise constantly. Along with lifelong performance properties under different and/or special user conditions, financial aspects such as production and material costs, as well as environment impact aspects are becoming increasingly important. All these are critical aspects to consider in the area of materials development. Geopolymers belong to the group of materials with increased interest due to the possibility of low CO_2-emission as well as low energy consumption, in comparison to cements and ceramics, respectively. The hardening process of geopolymers at room temperature may result in materials with ceramic-like properties, such as resistance against acids and high temperatures.

Geopolymeric binders or alkali-activated cements result from an alkaline activation of materials reactive in this respect. Concerning this ''reactive material'', there is a wide range of possible raw material. Beside primary resources like clay [1] (after thermal activation) and natural pozzolana [2] such as volcanic ashes, there is a considerable variety of secondary resources, like ashes [3] and slags [4], from different processes to use. In order to reduce environmental impacts and costs, industrial waste materials (secondary raw materials) were used for the development of geopolymers in this research project. In addition to Al_2O_3 and SiO_2, these secondary raw materials contain besides side phases like sulfates, chlorides, heavy metals also calcium compounds as main component. Therefore, the reaction products produces from the alkaline activation differ significantly. Slags which contain a lot of calcium oxide (>50%) in the reactive glass form C–S–H- and CAH-phases similar to such formed by

the hydration of portland cement, apart from tetrahedral aluminum incorporated into the dreierketten structure of the calcium silicate hydrates [5]. Pure aluminosilicate materials like metakaolin or aluminosilicate fly ashes form aluminosilicate polymer networks. Several raw materials, especially clays and natural pozzolana, contain about 5–20% CaO. Hence the question occurs: What happens in between these extremes of calcium content? Model mixtures showed that both reaction products (aluminosilicate and C–S–H-phases) coexist in different proportions depending on the concentration of the alkaline activator [6].

It is known that in principle the thermal resistance at temperatures >600 °C is low for normal portland cement binders and high for geopolymeric binders [2, 7]. Thus, thermal resistance may somehow correlate with the built reaction products. Several investigations were performed on the temperature stability and the phase conversions of geopolymers, which showed the dominance of the phase composition of the geopolymer [8–11]. Depending on the kind of alkali, kalsitite [8, 9] or nepheline [10] was found in geopolymers with low Si/Al ratios heated to 1,000 °C, and later transformed into leucite and carnegieite, respectively. Higher Si/Al ratios of the geopolymer, achieved by adding a silicate solution, generally led to less crystalline phases [11]. In fly ash based geopolymers, the partial transformation of nepheline into albite was measured [10]. The amount of silicate solution added highly influenced the form stability, as shown in [11] where small additions compensate shrinkage effects, but large additions led to expansion effects at a temperature >700 °C.

For a better understanding of the coherence between composition and properties, this investigation aimed at identifying the influence of calcium and its dosage on structure formation and property development—especially on structure stability at high temperatures up to 1,100 °C. The investigations were based on the built structure identified by ^{29}Si NMR spectroscopy and X-ray diffraction/Rietveld refinement, as well as strength performance after thermal treatment, length change behavior (also under load), and also the creep at high temperatures.

Investigation techniques

Materials, mixture, samples, and storage

The basis of the mixtures used in this investigation was an aluminosilicate hard coal fly ash (see Fig. 1) with a density of 2.61 g/cm^3 and a specific surface area of 2.9 m^2/g. The chemical composition of the fly ash is documented in Table 1 and was measured using common silicate chemistry methods. SiO_2 was determined gravimetrically after Soda-Borax pulping. The other oxides were measured in the pulping with hydrofluoric and nitric acid using ICP-OES. The phase composition of the fly ash was determined by XRD and Rietveld refinement, the ash was mixed with a standard material (10% ZnO) and milled in a slab mill. The results are shown in Fig. 2.

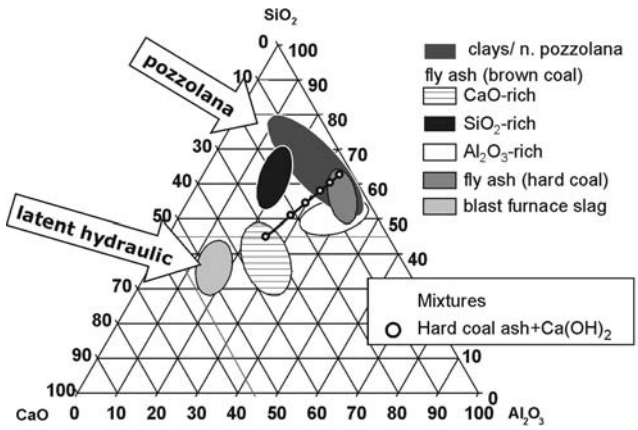

Fig. 1 Usable raw materials and their position in the CaO–SiO_2–Al_2O_3 ternary diagram compared to the generated mixtures

The fly ash was activated with 8 mol/L NaOH solution. In order to vary the calcium content in the mixtures, 0–20% of the fly ash was exchanged with very pure $Ca(OH)_2$-powder (CH). The composition of each mixture is documented in Table 2.

From the given mixtures samples of $10 \times 10 \times 60$ mm^3, $40 \times 40 \times 160$ mm^3, and $75 \times 110 \times 150$ mm^3 were cast and stored in molds at 40 °C and 100% r. h. for 3 days.

The de-molded samples were placed over water at room temperature in closed containers until the 24th day. Some samples were cut to the necessary size for the tests and softly dried at 40 °C (to avoid shrinkage cracks) until the 28th day of reaction. Strength measurements and the later temperature treatments of these samples were carried out in a dry state.

Table 1 Chemical composition of fly ash

wt.%	Fly ash
LOI	2.0
SiO_2	51.7
Al_2O_3	27.8
Fe_2O_3	6.6
CaO	2.8
MgO	3.2
TiO_2	1.3
K_2O	2.7
Na_2O	1.0

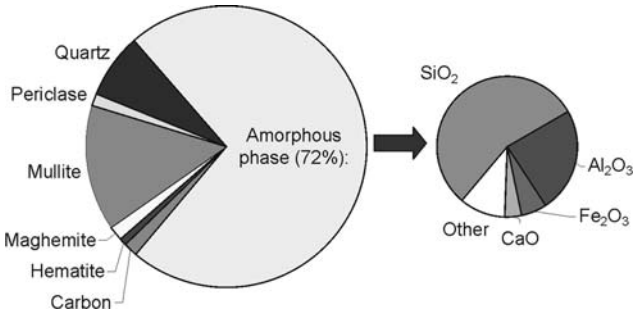

Fig. 2 Phase composition of the fly ash used and chemical composition of the amorphous phase

Table 2 Composition of mixtures

Mix labelling	CH-content (ref. to total solid material) %	Mixture composition (wt.%)			
		Fly ash	$Ca(OH)_2$	NaOH	H_2O
0%-CH	0	76.9	0.0	5.9	17.2
4%-CH	4	73.8	3.1	5.9	17.2
8%-CH	8	70.8	6.2	5.9	17.2
14%-CH	14	66.2	10.8	5.9	17.2
20%-CH	20	61.5	15.4	5.9	17.2

The small samples of $10 \times 10 \times 60$ mm^3 were stored over water at room temperature until the 28th and the 111th day of reaction, respectively. Strength measurements of these samples were carried out in moist state.

Structural investigation

Solid state NMR experiments were performed with a Bruker Avance™ 400 MHz WB, the resonance frequency of ^{29}Si and ^{27}Al was 79.52 and 104.29 MHz, respectively. For the ^{29}Si MAS NMR spectra the dried and ground samples were packed in 4 mm rotors and spun at 55 kHz under the magic angle. The chemical shifts were recorded relative to external tetramethylsilane (TMS). The single pulse technique was used, a typical number of scans was 12,000. For the ^{27}Al MAS NMR spectra the samples were packed in 4 mm rotors and spun at 15 kHz under the magic angle. The chemical shifts were recorded relative to external $Al(H_2O)_6^{3+}$. The single pulse technique was used, the number of scans was 1,000. The signal patterns of the spectra were deconvoluted with the Seasolve PeakFit® software using the Lorentz curve shape. Only material from $10 \times 10 \times 60$ mm^3 samples that had reacted for 28 days was analyzed.

In order to determine the X-Ray diffraction pattern, representative samples from the specimen after temperature treatment at 600, 800 and 1,000 °C were taken as well as from all specimen without high temperature treatment (small samples of $10 \times 10 \times 60$ mm^3 and large samples of $40 \times 40 \times 160$ mm^3). The (dry) material was ground and then mixed with a standard material (ZnO; about 10% per weight). The Rietveld Software Autoquant® was used to quantify the phase composition.

Measurement of reaction degree

The reaction degree was investigated by dissolving the dried and ground binders in hydrochloric acid following the instructions given in [12]. For the test, 1.00 g of the sample was suspended in 250 mL HCl (1:20) and homogenized for 3 h at room temperature. Afterwards the solution was filtered. The residue was washed, incinerated and burned at 1,000 °C to determine the non-soluble residue, which is equivalent to the non-reacted fly ash. Hence, the reaction degree was calculated. Moreover, the amount of reaction product (in respect to the binder mass dried) was determined as follows: The non-soluble residue (in respect to the dried sample) was subtracted from the amount of the XRD-amorphous content in order to get the amount of the amorphous reaction product. Hence the total amount of reaction product was calculated from it by adding the amount of the crystalline reaction products as determined by the X-ray.

Determination of strength and temperature performance

For investigating the high-temperature stability of the geopolymers, different testing methods were used. The methods, as well as samples sizes, treatment, and testing temperatures used are summarized in Table 3.

For the temperature treatment, the $40 \times 40 \times 160$ mm^3 samples were heated to 600, 800 and 1,000 °C, respectively, at 5 K/min, and held there for 60 min.

Bending-tensile and compressive strength tests were carried out at room temperature either after cooling from the temperature treatment or even without the temperature treatment. The bending-tensile strength (center point loading according to DIN EN 196-1) was measured on original samples, while the compressive strength was measured on the broken half's of the original samples from the bending-tensile strength test (also according to DIN EN 196-1 with a compression area of 1×2 cm^2 and 4×6 cm^2). Five samples were measured from the small samples ($10 \times 10 \times 60$ mm^3) and one or two from the large beams ($40 \times 40 \times 160$ mm^3). The compressive strength data were obtained from 10 single values from the $10 \times 10 \times 60$ mm^3 samples, and from 2 or 4 single values from $40 \times 40 \times 160$ mm^3 samples.

Table 3 Testing methods and parameters

Test	Sample size	Temperature treatment	Test Temperature
Bending-tensile strength; compressive strength	10 mm × 10 mm × 60 mm, 40 mm × 40 mm × 160 mm	40, 600, 800, 1,000 °C	20 °C
Dilation under load	Cylinder Ø = 50 mm, h = 50 mm	Approx. 1,100°C	20 °C—approx. 1,100 °C
Axial dilation	5 mm × 5 mm × 20 mm	20–1,100 °C	20–1,100 °C
Creep in compression	40 mm × 40 mm × 50 mm	Approx. 930 °C	Approx. 930 °C/25 h

To determine the thermal resistance of geopolymers various tests were involved. Dilation tests up to a temperature of 1,100 °C using the Linseis-dilatometer L75 were carried out on the $5 \times 5 \times 20$ mm^3 samples. Furthermore, dilation measurements under load were conducted according to DIN EN 993-8 (1997) ''refractoriness under load''. During this dilation test, a constant load of 0.05 MPa acted on the sample (cylinder; height and diameter = 50 mm). The test ''creep in compression'' (DIN EN 993-9; 1997) continued at the point where the dilation test under load ended. First the dilation under load was determined on $40 \times 40 \times 50$ mm^3 samples. The temperature and load is kept constant at about 930 °C for 25 h in order to determine the creep under compression.

Results and discussion

Treatment at moderate temperature

Structure

The XRD-results show that the reaction products of the fly ash binders are mainly X-ray amorphous, as expected. Small amounts of already crystalline alumosilicate could be detected as sodalite in small and large samples of all mixtures at 28 and 111 days. Some of the calcium hydroxide added did not initially react, and accumulated with increasing $Ca(OH)_2$-addition, but decreased with the reaction time. After 111 days of reaction, obvious amounts of crystalline C–S–H phases could be detected as reinhardtsbraunsite in the samples with 20% $Ca(OH)_2$. This confirms the statement in [13], significant amounts of calcium initially present may lead to C–S–H-formation. No CAH-phases could be found using XRD and Rietveld refinement. The results of the quantification are given in Table 4.

NMR spectroscopy gives clearer information about the reaction product, including the amorphous part. The ^{27}Al NMR results showed a spectra with only four-coordinated aluminum as a sharp peak around 60 ppm which can either be related to the tetrahedral aluminum incorporated into the silicate chains of the C–S–H-phase, or bonded in the aluminosilicate network. This difference appears more clearly in the ^{29}Si NMR spectra. Theoretically, silicate tetrahedra bonded in silicate chains can either be situated at the chain ends (Q_1; signal at –78 ppm ± 2 ppm) or in the middle (Q_2, signal at –85 ppm ± 2 ppm). If tetrahedral aluminum is incorporated into the silicate chain as a bridging tetrahedron, an additional peak can be seen at

Table 4 Phase composition of the hardened binders (large samples with $40 \times 40 \times 160$ mm^3 and small samples with $10 \times 10 \times 60$ mm^3)

wt.%	0% $Ca(OH)_2$			8% $Ca(OH)_2$			20% $Ca(OH)_2$		
	Large s.	Small s.		Large s.	Small s.		Large s.	Small s.	
	28 days	28 days	111 days	28 days	28 days	111 days	28 days	28 days	111 days
Amorphous	71	72	72	69	71	77	71	65	68
Calcite	–	–	–	–	–	–	5	–	–
Hematite	1	1	0	1	0	0	0	0	0
Maghemite	1	3	2	1	3	3	1	2	2
Mullite	15	14	14	12	13	11	8	10	9
Periclase	2	–	–	–	–	–	–	–	–
Portlandite	–	–	–	5	2	0	7	13	4
Quartz	8	7	8	7	7	7	5	6	6
Reinhardtsbraunsite	–	–	–	–	–	–	–	–	8
Sodalite	2	3	4	4	4	2	3	4	3
Sum	100	100	100	100	100	100	100	100	100

–82 ppm ± 2 ppm (Q_2(1Al)) [5, 14]. Amorphous aluminosilicate networks and zeolites are built by a network of silicate and aluminate tetrahedra, which are connected at all four corners to other tetrahedra. Therefore five possible peaks of silicate tetrahedron Q_4, which are connected to either zero, one, two, three or four aluminate tetrahedra, might be detectable in the spectra between –110 and –85 ppm [15, 16].

The results of the ^{29}Si NMR spectroscopy of the fly ash binders at the age of 28 days are given in Fig. 3. The broad fly ash hump centered at about –100 ppm indicates a very low reaction degree. The main peak of the reaction products are found between –70 and –90 ppm. As the calcium content increases, the center of this peak seems to shift from –87 to –85 ppm, connected with a spreading/broadening. If the peak at about –87 ppm of the $Ca(OH)_2$-free sample is labeled to be the Q_4(4Al)-signal of the built aluminosilicate network, then the shifting might be caused by the overlapping of this peak with the Q_2-signals (at about –84 ppm) from the C–S–H-phase. A deconvolution was determined based on these considerations. The spectra of the unreacted fly ash was fitted as two separate peaks, one broad peak of the glass centered at about –102 ppm and a second of the crystalline mullite at –88 ppm [17]. The parameters of these peaks (center and width) was used to fit the $Ca(OH)_2$-free sample. The results are shown in Fig. 4. Four peaks of the aluminosilicate network were then fitted with centers at –86.6 ppm/Q_4(4Al), –93 ppm/Q_4(3Al), –96 ppm/Q_4(2Al) and –100 ppm/Q_4(1Al). This deconvolution used peaks with a Lorentz shape and identical peak widths.

The parameters determined by this procedure were used to deconvolute the 20% $Ca(OH)_2$-sample using known peak positions of C–S–H from [14]. The results are shown in Fig. 5. The molar ratio Si/Al of the aluminosilicate network should be slightly larger than 1.0 because of the detected signals up to –100 ppm, indicating not only aluminum tetrahedra in the next nearest neighborhood. It should be mentioned that such a approach contains imponderableness due to a

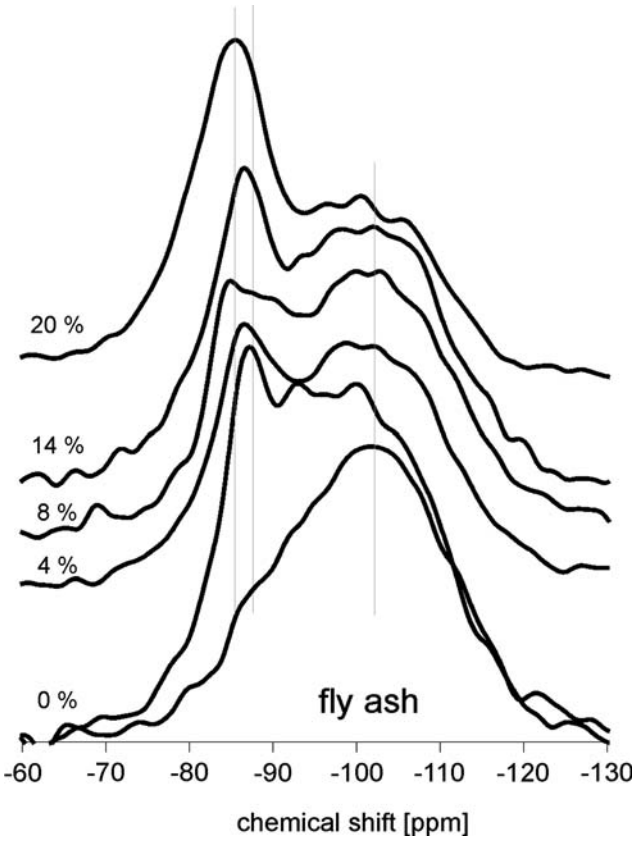

Fig. 3 Comparison of the ^{29}Si NMR spectra of all fly ash binders after 28 days hardening at room temperature (small samples $10 \times 10 \times 60$ mm^3); vertical lines mark the position of the main peak of fly ash, 0% and 20%- $Ca(OH)_2$-mixture

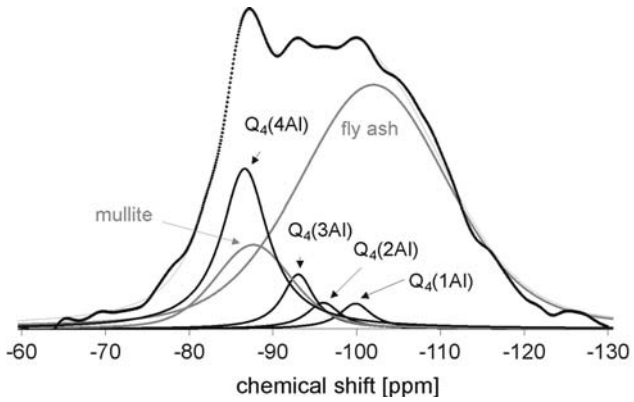

Fig. 4 Peak separation of the ^{29}Si NMR spectra of fly ash binders with 0% $Ca(OH)_2$ content

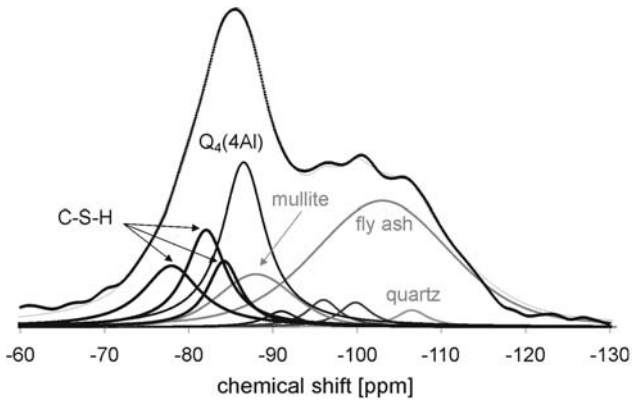

Fig. 5 Peak separation of the ^{29}Si NMR spectra of fly ash binders with 20% $Ca(OH)_2$ content

possibly selective dissolution of the fly ash glass that has not yet been proven. The strong overlapping peaks and the high amount of non-reacted fly ash might yield to equivocal quantifications of the determined peaks. Extremely overlapping peaks of the $Q_4(4Al)$- and the Q_2-signal from aluminosilicate network and C–S–H-phase both combine to the main broad peak at –86 ppm. Therefore to avoid over interpretation, an exact quantification was not performed. Nevertheless, it can be concluded that both—aluminosilicate phases and C–S–H-phases—can be proved in the matrix of the calcium containing samples, especially at high calcium hydroxide contents of about 20%.

Reaction degree

The impact of the calcium content on the reaction degree can be seen in Table 5. With increasing calcium content the amount of reacted fly ash increases from less than 20% up to 40%. In comparing the reaction degrees of the small and the large samples, it can be seen that the large samples achieved higher values after 28 days of reaction, in comparison to small samples after 111 days of reaction.

The amount of reaction product with respect to the dry sample increased from 14 wt.% up to 40 wt.% by adding calcium hydroxide (small samples after 111 days of reaction). The other samples show a similar trend. The values of the large samples after 28 days are again comparable to the values of the small samples after 111 days of reaction.

This fact can be explained by a longer storage of heat in the larger sample coupled with the final drying of the larger sample, which result in a higher activation energy and therefore a higher reaction degree.

Aside from the impact of the calcium addition, the improvement of the reaction degree might be related to the higher Na/Al ratio in the samples. The NaOH concentration was kept constant for all mixtures to guarantee the same dissolution rate. However, during the reaction, a higher amount of alkali (and the sum of alkali and earth alkali) might influence the charge compensation of the aluminosilicate network, and thus the reaction degree.

Table 5 Reaction degree (RD; reacted fly ash in %) and content of reaction product (RP; in respect to the dry sample, % by weight)

	Large samples		Small samples			
	28 days		28 days		111 days	
	RD %	RP wt.%	RD %	RP wt.%	RD %	RP wt.%
0%-$Ca(OH)_2$	28	10	n.d.	n.d.	29	14
8%-$Ca(OH)_2$	39	24	20	9	33	27
20%-$Ca(OH)_2$	44	36	36	23	42	40

Strength performance

Figure 6 shows the strength of the binders after 28 and 111 days of reaction. For the strength tests on small samples ($10 \times 10 \times 60$ mm^3) after 28 days, it was seen that a small calcium hydroxide addition led to a slightly worse strength compared to pure fly ash samples, this agrees with reference [18]. After 28 days, the more the $Ca(OH)_2$-content is increased, the higher the strength will become, which in turn correlates with the amount of reaction products formed. For the tests on small samples after 111 days, generally higher strength values were evident due to higher reaction degrees. Here, any addition of calcium lead to a much higher strength in comparison with samples with no $Ca(OH)_2$ addition; an optimal $Ca(OH)_2$-content of 8% became clear. Surprisingly though, this does not correlate with the amount of built reaction product. This could mean that the built reaction product has a much stronger structure.

The large samples ($40 \times 40 \times 160$ mm^3) showed the same trend after 28 days of reaction, nevertheless after 111 days, the strength values of $Ca(OH)_2$-containing large samples were about 5–10 MPa lower compared to the small samples. Higher temperatures in the early reaction stage and drying at 40 °C before testing led to a curing and faster reaction in the larger samples.

As seen from the density measurements, the matrix becomes more compact and dense with increasing contents of calcium hydroxide, as shown in SEM images in Fig. 7. It should also be mentioned that there is a homogeneous distribution of calcium in the matrix, as proven by SEM element mapping.

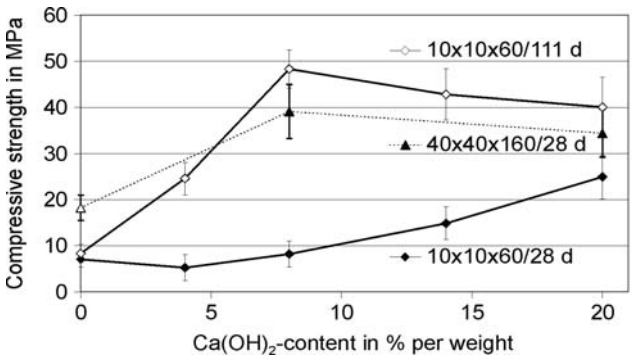

Fig. 6 Compressive strength of fly ash binders as a function of $Ca(OH)_2$-content, sample size, and sample age; treatment temperature 40 °C

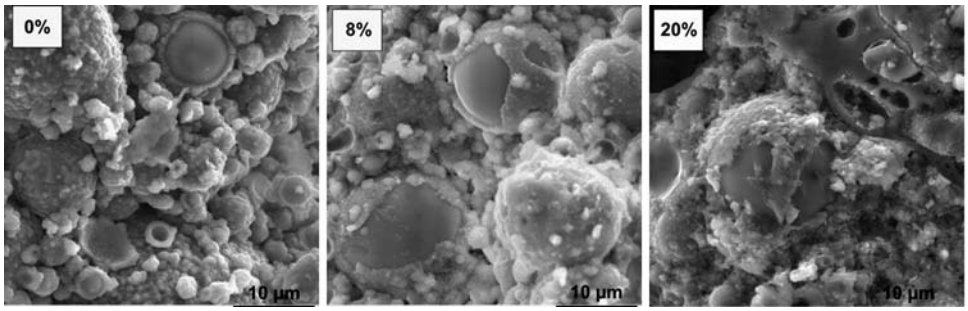

Fig. 7 SEM image of fly ash binders with 0, 8, and 20% $Ca(OH)_2$ content after treatment at room temperature

Treatment at high temperature

Structure after temperature treatment

Figure 8 shows the result of XRD investigations on large samples with 8% $Ca(OH)_2$ after treatment at different temperatures. Samples treated at 600 °C are mainly amorphous, with no significant difference in the amounts compared with the material treated at room temperature. Only a small amount of sodalite content was detected. From 600 °C to 800 °C the amount of the amorphous phase decreases (Fig. 8). At 800 °C, the first new phase formations can be identified. All series (0%, 8%, and 20% $Ca(OH)_2$ content) contain nepheline ($NaAlSiO_4$), which is formed due to the sodalite-decomposition as well as from amorphous alumosilicate counterparts [19]. Gehlenite ($Ca_2Al_2SiO_7$) was found in all calcium containing samples and was developed due to the decomposition of C–S–H and/or zeolites. Some leftovers from the fly ash such as quartz and mullite ($Al_6Si_2O_{13}$) were also found (Fig. 8). In the X-ray diffraction graph at 1,000 °C the amorphous phase is no longer recognizable (Fig. 8). Fe_2O_3 (maghemite; hematite) and nepheline were found after treatment at 1,000 °C. In general, if silicon dioxide is available at such a high temperature, nepheline is no longer stable and feldspar will form. The amount of calcium available causes different types of feldspar to form (Fig. 9): samples with no or little $Ca(OH)_2$-addition form Na-feldspar such as albite ($NaAlSi_3O_8$; Ca-rich) and samples with a lot of $Ca(OH)_2$ form Ca-feldspars such as anorthite ($Ca(AlSiO_4)_2$; Na-rich).

The results of the quantitative phase analysis by Rietveld refinement are given in Table 6. The results show the decrease in degree of the amorphous phase with increasing temperature treatment. The sample with no addition of $Ca(OH)_2$ showed the highest degree of amorphous phase at each temperature, which is stable and in charge of the strength. At room temperature, the sample with 8% $Ca(OH)_2$ showed the highest amount of sodalite, and at 800 °C and 1,000 °C the highest amounts of nepheline and feldspar, respectively. Even after a temperature treatment at 1,000 °C there was still nepheline left, a small amount present in the sample with no $Ca(OH)_2$ addition, and a reasonable amount in the 8% $Ca(OH)_2$ sample, and a rather large amount in the sample with 20% $Ca(OH)_2$ addition. One reason to explain this could be that all the mullite and quartz were needed to form the large amount of gehlenite.

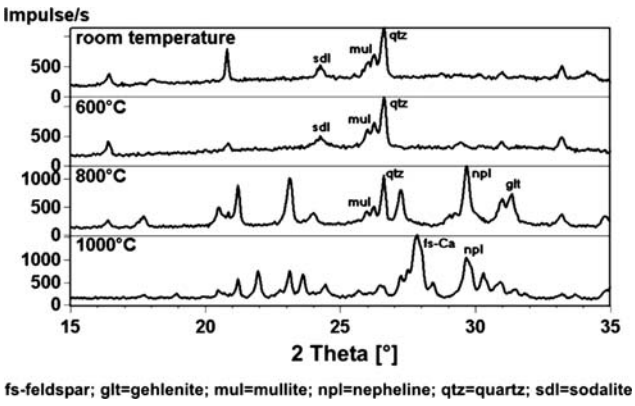

Fig. 8 XRD curves showing the influence of treatment temperature on phase composition; example: 8% $Ca(OH)_2$-sample

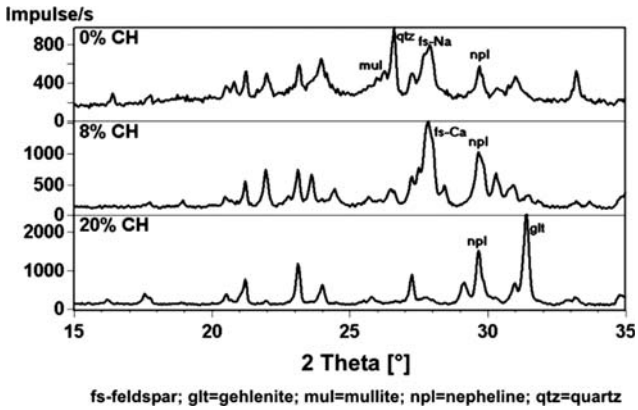

Fig. 9 XRD curves showing the influence of $Ca(OH)_2$-addition; treatment temperature: 1,000 °C

Table 6 Phase composition of the thermally treated binders

Wt.%	0% $Ca(OH)_2$			8% $Ca(OH)_2$			20% $Ca(OH)_2$		
	No	800 °C	1,000 °C	No	800 °C	1,000 °C	No	800°C	1,000°C
Amorphous	71	64	60	69	44	12	71	39	22
Albite	–	–	17	–	–	–	–	–	–
Anorthite	–	–	–	–	–	55	–	–	4
Calcite	–	–	–	–	–	–	5	–	–
Gehlenite	–	–	–	–	7	–	–	20	32
Hematite	1	1	2	1	1	0	0	1	0
Maghemite	1	3	2	1	2	6	1	1	2
Mullite	15	14	5	12	8	–	8	5	–
Nepheline	–	9	9	–	33	25	–	27	40
Periclase	2	–	–	–	–	–	–	–	–
Portlandite	–	–	–	5	–	–	7	–	–
Quartz	8	7	5	7	5	1	5	6	–
Sodalite	2	2	–	4	–	–	3	–	–
Sum	100	100	100	100	100	100	100	100	100

Refractory tests

The results of the dilation test without load are presented in Fig. 10. The results support the theory of the optimal calcium content. An addition of 8% calcium hydroxide led to the smallest shrinkage, up to temperature of 1,050 °C. The samples with the highest amount of calcium hydroxide added had the best performance at 1,100 °C—with an acceptable shrinkage of <2%.

The results of the dilation test under load, which are shown in Fig. 11, emphasize the optimal amount of 8% $Ca(OH)_2$. Here, the threshold for an acceptable shrinkage of 2% was reached at about 1,050 °C, whereas the mixtures with no addition or an addition of 20% $Ca(OH)_2$ reached a limit at about 810 °C or 960 °C, respectively.

Figure 12 shows the results of the ''creep in compression'' test. The sample with 8% $Ca(OH)_2$ did not show further shrinkage beyond 2% during 25 h of load at a temperature of 930 °C, in contrast to the sample with 20% calcium hydroxide which shrank slightly below 2%, and to the sample without $Ca(OH)_2$-addition which shrank more than 6%.

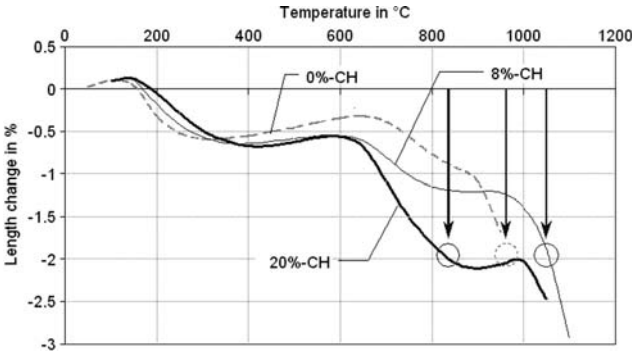

Fig. 11 Results of dilation test under load

Fig. 10 Results of dilation tests without load

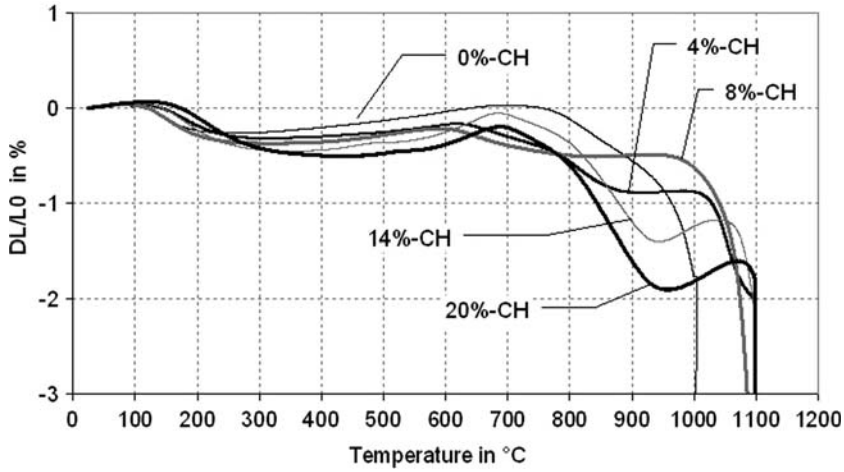

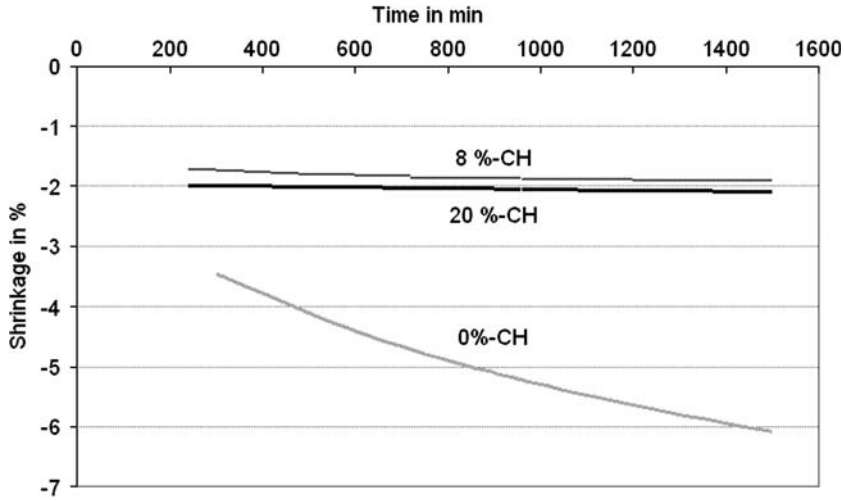

Fig. 12 Results of ''creep in compression'' test

The formation of more crystalline products during the temperature treatment due to an 8%-$Ca(OH)_2$-addition led to better temperature performance compared with a calcium free sample. At higher $Ca(OH)_2$-contents, the samples were susceptible to higher temperature due to the reduction of the melting point by the calcium.

Strength after temperature treatment

The results of the sample strength measured after temperature treatments of 600, 800 and 1,000 °C are given in Figs. 13 and 14. The strength of the sample without $Ca(OH)_2$-addition increases after a temperature treatment of 800 and 1,000 °C due to shrinkage and densification. The strength of the sample with 8% $Ca(OH)_2$-addition is similar; only the compressive strength after a 600 °C treatment decreases slightly, as opposed to the sample with 20% $Ca(OH)_2$-addition. The highest strength is shown after 600 °C, the strength after 800 °C and 1,000 °C treatment are either similar or lower than the strength before temperature treatment.

Therefore, an optimal calcium hydroxide content of 8% is still valid.

The same optimal extent determined from compressive strength test was also determined in bending-tensile strength tests (Fig. 14). The strength of the samples with no and 8% $Ca(OH)_2$-addition after treatment at 800 and 1,000 °C was higher than the strength without temperature treatment. This is contrary to the strength after 600 °C, which was lower than

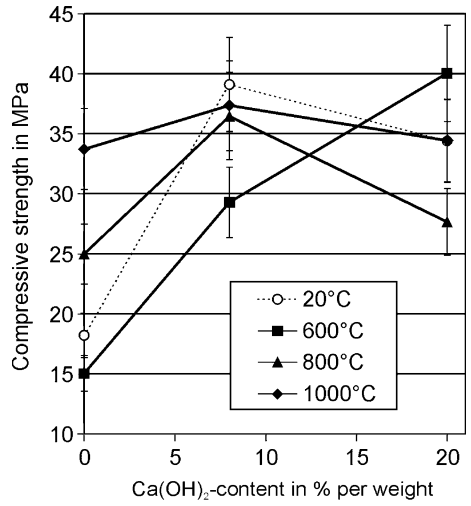

Fig. 13 Compressive strength as a function of $Ca(OH)_2$-content, tested at 20 °C after temperature treatment ($40 \times 40 \times 160$ mm^3 samples)

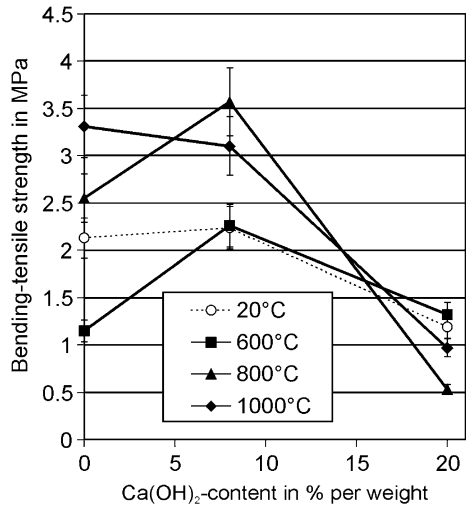

Fig. 14 Bending-tensile strength as a function of $Ca(OH)_2$-content, tested at 20 °C after temperature treatment ($40 \times 40 \times 160$ mm^3 samples)

the strength without temperature treatment. The bending tensile strength of the sample with 20% $Ca(OH)_2$-addition after every temperature treatment was low compared to non-treated samples.

The correlation between structure and strength became visible. The addition of a certain amount of calcium led to formation of more crystalline phases and thus to higher strength. Also heavy shrinkage and thus cracking became evident on samples with high amounts of calcium, which result in lower strength values.

Conclusion

This study investigated the influence of calcium content on structure and the thermal properties of fly ash based geopolymers. Varying amounts of calcium content in the mixtures were obtained by adding pure solid calcium hydroxide to the fly ash. Sodium hydroxide solution was used for activation.

Investigations at room temperature—as expected—gave evidence of mainly X-ray amorphous reaction products. It can be concluded that this X-ray amorphous phase includes both aluminosilicate and C–S–H-phases, which coexist as reaction products in samples with high calcium content. Along with a respectable amount of C–S–H-phases, samples with very high calcium content (20% substitution of fly ash) still contained a decent amount of zeolitic phases, as proven by X-ray diffraction and NMR spectroscopy.

With prolonged reaction time and increased calcium content the samples showed an increased reaction degree and thus higher strength. The mixture with 8% calcium hydroxide reached maximum strength values, demonstrating its extraordinary performance.

Depending on the calcium content, the phase transformation at high temperatures, and thus the strength after temperature treatment, was impacted. The following can be stated:

– Investigations on heat treated samples showed similar results in XRD and Rietveld refinement; the detected amount of sodalite with temperature treatment was less compared to room temperature treatment. Sodalite and amorphous aluminosilicates that were formed during the first stage were transformed into nepheline at temperatures higher than 600 °C. Similarly, the gehlenite phase could be formed in calcium containing samples. Due to this, the samples had a denser structure and shrinkage was detected.
– Temperature increase causes the nepheline to no longer be stable in its coexistence with available silicate, which comes from quartz and mullite in the calcium free sample. As a result, albite forms. If a moderate amount of calcium is available (for instance, if it is bonded in zeolitic structures) then the nepheline will decompose, and calcium feldspars of the plagioclase group are formed. Such decomposition could not be detected in samples with lots of calcium, which therefore showed an increasing amount of nepheline as well as gehlenite. The thermal properties reflect the different mineral forming and conversion processes.

Samples with 8% calcium hydroxide addition contained the highest amounts of nepheline at 800 °C and of feldspar at 1,000 °C. Hence these samples possess the highest strength and lowest shrinkage. The latter was proven by means of dilation tests with and without load, as well as by creep under compression tests. All results combine to demonstrate an optimal $Ca(OH)_2$-content at about 8% substitution of fly ash per weight, which showed good performance at room temperature as well as at high temperatures. This material is mainly composed of aluminosilicate network phases and few calcium silicate hydrate phases, which seem to be in a good coexistence. Additionally, it can be concluded that calcium acts as a reaction germ at a certain amount which quickens the reaction to more structure-forming products, and thus results in higher strength.

Acknowledgement The project is supported by the German foundation VolkswagenStiftung. To them the authors are deeply grateful. The research team wants also to thank Dr. Erica Brendler, TU Bergakademie Freiberg, for the NMR measurements, and Mr. Torsten Westphal, TU Bergakademie Freiberg, for XRD and Rietveld analyses.

References

1. Buchwald A, Kaps Ch (2002) In: Luckey GC (ed) Geopolymer. Publisher: Melbourne, Australia
2. Davidovits J, Buzzi L, Rocher P, Gimeno D, Marini C, Tocco S (1999) In: Davidovits J et al (ed) Proceedings of the second international conference geopolymere 99, pp 83–96
3. Fernandez-Jimenez A, Palomo A (2003) In: Grieve G, Owens G (eds) Proceedings of 11th international congress on the chemistry of cement (ICCC). Durban, South Africa, pp 1332–1339
4. Talling B, Brandstetr J (1989) In: V.M. Malhotra (ed) Proceedings of the 3rd int. conf. of fly ash, silica fume, slag and natural pozzolans in concrete. Publisher, pp 1519–1545
5. Schilling PJ, Butler LG, Roy A, Eaton HC (1994) J Am Ceram Soc 77(9):2363

6. Palomo A, Blanco-Varela T, Alonso S, Granizo L (2003) In: Grieve G, Owens G (eds) Proceedings of 11th international congress on the chemistry of cement (ICCC). Publisher, Durban, South Africa, pp 425–434
7. Davidovits J (1991) J Thermal Anal 37:1633
8. Comrie DC, Kriven WM (2003) In: American Ceramic Society (ed) Advances in ceramic matrix composites IX: proceedings of the Ceramic matrix . Ceramic transactions, vol 153, pp 211–225
9. Barbosa VFF, MacKenzie KJD (2003) Mater Lett 57:1477
10. Krivenko PV, Kovalchuk GYu (2002) In: Luckey GC (ed) Geopolymer. Publisher, Melbourne, Australia
11. Duxson P, Luckey GC, van Deventer JSJ (2006) In: Davidovits J (ed) Geopolymer, green chemistry and sustainable development solutions. Proceedings of the world congress of geopolymer 2005, St. Quentin, France, pp 189–194
12. Criado M, Palomo A, Fernández-Jiménez A (2005) Fuel 84:2048
13. Yip CK, Lukey GC, van Deventer JSJ (2005) Cement Concrete Res 35:1688
14. Sun GK, Francis Young J, James Kirkpatrick R (2006) Cement Concrete Res 36:18
15. Klinowski J (1984) J Prog NMR Spectros 16:237
16. Engelhardth G, Michel D (1987) High resolution solid state NMR of silicates and zeolites. Ed. John Wiley and sons
17. Mackenzie KJD, Smith ME (2002) In: Cahn RW (ed) Multinuclear solid-state NMR of inorganic materials, Pergamon materials series. Pergamon, Amsterdam
18. Lee WKW, van Deventer JSJ (2002) Cement Concrete Res 32:577
19. Dimitrijevic R, Dondur V, Vulic P, Markovic S, Macura S (2004) J Phys Chem Solids 65:1623